Structures 79 (2025) 109416

Contents lists available at ScienceDirect

Structures

journal homepage: www.elsevier.com/locate/istruc

Optimal design and performance assessment of enhanced TMDI with tuned inerter-based dampers

Xiaoyu Bai [a], Qigang Liang [a,b,*], Luyu Li [a,b], Breiffni Fitzgerald [c], Jinping Ou [a,b]

[a] School of Infrastructure Engineering, Dalian University of Technology, Liaoning 116024, China
[b] State Key Laboratory of Coastal and Offshore Engineering, Dalian University of Technology, Liaoning 116024, China
[c] School of Engineering, Trinity College Dublin, Dublin D02 PN40, Ireland

A R T I C L E I N F O

Keywords:
Tuned mass-damper-inerter
Tuned inerter-based dampers
Fixed-point theory
Optimal design
Closed-form solution
Base isolation system

A B S T R A C T

To enhance the control performance of a tuned mass damper (TMD) while reducing the tuned mass demand, this paper introduces a novel vibration mitigation strategy: the tuned mass-damper-inerter (TMDI) enhanced by tuned inerter-based dampers (TMDI-TIBD). This study formulates equations of motion and transfer functions for single-degree-of-freedom (SDOF) structures equipped with TMDI-TIBD. Closed-form optimal design formulas are derived using fixed-point theory to minimize displacement and acceleration amplitudes. The control performance of TMDI-TIBD is evaluated through comparative analyses of structural responses, tuned mass stroke, and detuning effect, compared to the TMD and TMDI strategies. TMDI-TIBD is applied to a base-isolated system (BIS) to enhance the vibration isolation performance, with time-history responses compared under seismic excitation. In general, the proposed TMDI-TIBD maintains higher control performance, stronger control robustness, and lower tuned mass demand compared to conventional TMD. In addition, TMDI-TIBD shows a significant improvement in control performance and robustness for structures subjected to harmonic excitation compared to TMDI, regardless of the slightly amplified tuned mass stroke. In summary, TMDI-TIBD leverages the triple-tuning effect of TIBD-enhanced TMD and the mass amplification effect of the inerter, which is a more flexible and adaptable strategy for vibration control of different types of structures.

1. Introduction

Tuned mass dampers (TMDs) are widely used dynamic vibration absorbers (DVAs) in the field of vibration control [1–4]. The classical linear TMD achieves optimal control of the structure through the optimal design of its tuning stiffness and damping parameters. The parameter design method based on fixed-point theory originally presented by Den Hartog is widely applied in the parameter design of TMD devices [2,5]. Existing research on the innovation of linear TMD devices mainly focuses on the implementation of stiffness and damping elements, such as electromechanical damping TMDs [6,7]. Additionally, several new forms of TMD have been developed based on linear TMDs, such as pounding TMDs that achieve limiting and energy dissipation through boundary constraints [8], particle TMDs that dissipate energy through particle collisions [9], pendulum TMDs designed with specific motion trajectories [10], and TMDs with the characteristic of clutching inertia (CTMD) [11]. Although these nonlinear TMDs show improved practicality compared to linear TMDs, they do not significantly surpass linear TMDs in terms of control performance and often achieve only comparable results.

The emergence of the inerter [12] and other inerter-based devices [13–17] has provided new avenues for the development of TMD. By incorporating a mixed model of an inerter with springs and damping units into the classical TMD, the replacement of the damping unit forms a new tuning system that has been proven to exhibit better vibration reduction performance and robustness. Garrido et al. [18] first introduced the tuned viscous mass damper (TVMD) [14] into the classical TMD, forming a rotational inertia double-tuned mass damper system (RIDTMD), and obtained the optimal parameters of the RIDTMD through H_∞ norm optimization. Under optimally designed parameters, RIDTMD demonstrates a triple-peak tuning effect, showing not only better vibration suppression performance compared to classical TMDs but also significantly increased control bandwidth. Subsequently, Hu et al. [19] studied the performance of the H_2 norm and the H_∞ norm for four types of three-unit configurations that replace the damping unit of the

* Corresponding author at: School of Infrastructure Engineering, Dalian University of Technology, Liaoning 116024, China
Email address: lqg@dlut.edu.cn (Q. Liang).

https://doi.org/10.1016/j.istruc.2025.109416
Received 11 February 2025; Received in revised form 9 June 2025; Accepted 9 June 2025

classical TMD from both theoretical and numerical optimization perspectives, indicating that the new configurations could improve control effectiveness by 20 % compared to the classical TMDs. Furthermore, Barredo et al. [20] provided analytical solutions for optimal parameters of inerter-based dynamic vibration absorbers (IDVA) formed by three-unit configurations based on extended fixed-point theory. The efficiency of RIDTMD installed on different engineering structures to mitigate vibrations has been verified, including on bridges [21], transmission towers [22], and floating offshore wind turbines [23]. In addition to integrating the inerter into TMDs, directly utilizing the inerter as a connecting unit between the mass of the classical TMD and the ground or fixed ends is also an effective method to enhance the performance of classical TMDs. Marian and Giaralis [24] first proposed the concept of tuned mass-damper-inerter (TMDI), providing analytical solutions for optimal parameters of TMDI based on variance response control of the primary structure subjected to ground excitation. This scheme significantly reduces the mass requirement of the TMD by utilizing the mass amplification effect of the inerter. The experimental study verifies that the TMDI remains effective when modeled with nonlinear behavior, in addition to the idealized case [25]. In a 74-story structure, the TMDI installed on the top floor is connected to different floors below, reducing the tuned mass requirement by 50 %, and this scheme provides better control for higher-order modal responses [26]. Since the inerter in TMDI is connected to the ground, it can maximize the mass amplification effect, and the TMDI scheme has also been introduced into the base-isolated system (BIS), reducing the response of the isolation floor without significant adverse impact on the superstructure [27,28]. From a constructional perspective, a well-established strategy involves the use of rotational inertia achieved through a ball-screw mechanism [29], while structural seismic protection can be further enhanced through the integration of the clutch [30–32]. Hydraulic inerters [33] and electromagnetic inerters [34] also warrant considerable attention when cost is not a limiting factor. The effectiveness of TMDI with rotational inertia and hydraulic inertia in enhancing BIS has further been verified through experimental studies [35,36]. Additionally, several variants of TMDI have emerged [37–45]. Overall, the inerter has significantly enhanced traditional TMDs in terms of control performance, robustness, and reduction of tuned mass requirements.

Inspired by existing research, this paper proposes a novel TMDI scheme enhanced by tuned inerter-based dampers (TMDI-TIBD) to improve the control performance of the conventional TMD while reducing the tuned mass requirement. This innovation also provides a significant advancement in control robustness owing to the triple-tuning effect. Although TMDI-TIBD can achieve an identical effect to the large-mass IDVA when the inerter is fixed to the ground, the introduction of the inerter will influence the responses of higher modes in multi-degree-of-freedom (MDOF) structures, which is a characteristic that IDVA and TMD lack. When the primary structure is excited by a harmonic load, the optimal parameters of TMDI can be derived by replacing the tuned mass ratio with the sum of the tuned mass ratio and inertance-mass ratio [26], and therefore, the optimal parameters of TMDI-TIBD can be derived by the same operation. Nonetheless, the optimal parameters of TMDI-TIBD are still unexplored when the structure is subjected to harmonic excitation.

This paper focuses on the theoretical analysis of TMDI-TIBD and the outline is as follows. First, the equations of motion and transfer functions of a single-degree-of-freedom (SDOF) structure equipped with the proposed TMDI-TIBD control strategy are established. Second, the optimal design parameters of TMDI-TIBD based on fixed-point theory are derived to minimize the displacement and acceleration amplitudes under harmonic excitation. Third, the TMDI-TIBD's control performance is evaluated comprehensively by analyzing the responses of the primary structure, the tuned mass stroke, and the detuning effect. Finally, the vibration isolation performance of the TMDI-TIBD-enhanced BIS subjected to seismic excitation is further investigated.

2. Modeling of TMDI-TIBD in SDOF structures

The proposed TMDI enhanced by a tuned inerter-based damper (referred to as TMDI-TIBD) is formed by replacing the damping unit of the TMDI with TIBD, as illustrated in Fig. 1. TIBD includes TVMD and tuned-inerter-damper (TID) [13]; therefore, TMDI-TIBD is referred to as TMDI-TVMD or TMDI-TID when TVMD or TID is used. Alternatively, under the condition $m_1 = 0$ or $b_1 = 0$ (as shown in Fig. 1(c)), TMDI-TIBD can be simplified into a two-terminal or a single-terminal damper.

2.1. Equation of motion

When a structure with TMDI-TIBD is excited by ground acceleration $\ddot{x}_g$, the equation of motion (EOM) can be expressed as follows:

$$\mathbf{M}\ddot{\mathbf{x}} + \mathbf{C}\dot{\mathbf{x}} + \mathbf{K}\mathbf{x} = -\mathbf{M}_{\mathbf{I}}\ddot{x}_g \tag{1}$$

where $\mathbf{x} = [x, x_1, x_t]^T$ is the displacement vector representing the displacement of the primary structure, tuned mass, and the TIBD. $\mathbf{M}$, $\mathbf{K}$, and $\mathbf{C}$ are the mass, stiffness, and damping matrices of the controlled structure, respectively; $\mathbf{M}_{\mathbf{I}} = \left[m, m_1, 0\right]^{\mathrm{T}}$ is the column vector corresponding to the excitation.

For the TMDI-TVMD controlled structure, the mass, damping, and stiffness matrices are defined as:

$$\mathbf{M} = \begin{bmatrix} m & 0 & 0 \\ 0 & m_1 + b_1 + b_t & -b_t \\ 0 & -b_t & b_t \end{bmatrix}, \quad \mathbf{C} = \begin{bmatrix} c & 0 & 0 \\ 0 & c_t & -c_t \\ 0 & -c_t & c_t \end{bmatrix},$$

$$\mathbf{K} = \begin{bmatrix} k + k_1 + k_t & -k_1 & -k_t \\ -k_1 & k_1 & 0 \\ -k_t & 0 & k_t \end{bmatrix} \tag{2}$$

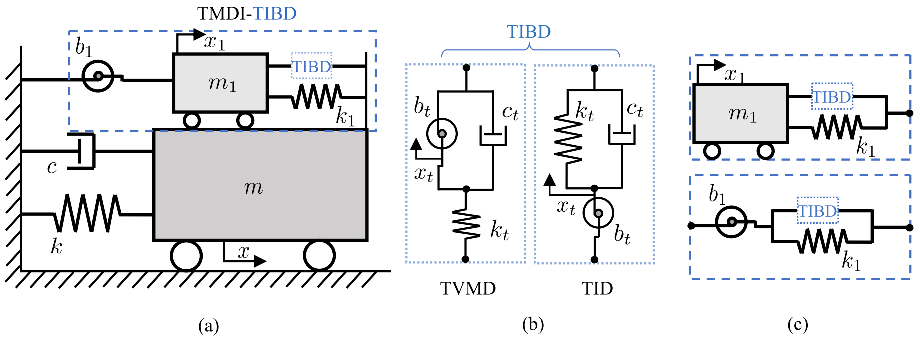

Fig. 1. Analysis model of (a) TMDI-TIBD in an SDOF; (b) TIBD in TMDI-TIBD; (c) variants of TMDI-TIBD.

Table 1
Notations.

Variable	Definition	Interpretation
f_1	$f_1 = \omega_1/\omega$	Frequency ratio of TMDI
f_t	$f_t = \omega_t/\omega_1$	Frequency ratio of tuned inerter-based dampers
ζ_t	$\zeta_t = \dfrac{c_t}{2\sqrt{b_t k_t}}$	Damping ratio of tuned inerter-based dampers
β_t	$\beta_t = \dfrac{b_t}{m_1 + b_1}$	Inertance-mass ratio of tuned inerter-based dampers
β_1	$\beta_1 = b_1/m$	Inertance-mass ratio of TMDI and primary structure
μ	$\mu = m_1/m$	Mass ratio of the tuned mass and primary structure
ω	$\omega = \sqrt{k/m}$	Circular frequency of the primary structure
ξ	$\xi = \dfrac{c}{2\sqrt{mk}}$	Damping ratio of the primary structure
ω_1	$\omega_1 = \sqrt{\dfrac{k_1}{m_1 + b_1}}$	Circular frequency of TMDI
ω_t	$\omega_t = \sqrt{k_t/b_t}$	Circular frequency of tuned inerter-based dampers

Similarly, for the TMDI-TID controlled structure, the mass, damping, and stiffness matrices are defined as:

$$\mathbf{M} = \begin{bmatrix} m+b_t & 0 & -b_t \\ 0 & m_1+b_1 & 0 \\ -b_t & 0 & b_t \end{bmatrix}, \quad \mathbf{C} = \begin{bmatrix} c & 0 & 0 \\ 0 & c_t & -c_t \\ 0 & -c_t & c_t \end{bmatrix},$$
$$\mathbf{K} = \begin{bmatrix} k+k_1 & -k_1 & 0 \\ -k_1 & k_1+k_t & -k_t \\ 0 & -k_t & k_t \end{bmatrix} \tag{3}$$

where m, k, and c are the mass, stiffness, and damping of the primary structure; m_1, k_1, and b_1 are the mass, stiffness, and inertance of the TMDI component; b_t, k_t, and c_t represent the inertance, stiffness, and damping coefficients of the TIBD.

2.2. Transfer functions

2.2.1. Transfer functions in frequency-domain expression

When the structure is excited by a sinusoidal ground motion $\ddot{x}_g = A_0 e^{iwt}$, the steady-state displacement follows $x = Ue^{iwt}$. Therefore, the dimensionless transfer function of structural displacement can be defined as

$$H_d(\mu, \beta_1, \beta_t, f_1, f_t, \gamma) = \frac{U}{A_0} = \frac{A+Bi}{C+Di}, \tag{4}$$

and the amplitude of this transfer function is given by

$$|H_d(\mu, \beta_1, \beta_t, f_1, f_t, \gamma)| = \sqrt{\frac{A^2+B^2}{C^2+D^2}}, \tag{5}$$

where γ is the frequency ratio of external excitation to the structural natural frequency; $\mu, \beta_1, \beta_t, f_1, f_t$ are the design parameters of TMDI-TIBD and their definitions are listed in Table 1. The expressions of A, B, C, and D can be found in Appendix A.

According to the relationship between relative acceleration and displacement in the frequency domain, the transfer function of structural relative acceleration and the corresponding amplitude is defined as

$$H_a(\mu, \beta_1, \beta_t, f_1, f_t, \gamma) = -\gamma^2 H_d, \quad |H_a(\mu, \beta_1, \beta_t, f_1, f_t, \gamma)| = |\gamma^2 H_d|. \tag{6}$$

2.2.2. Transfer functions in state-space form

Numerical optimization usually yields accurate results when considering more factors in the optimal design process, such as structural damping, which can be incorporated into the transfer function via the state-space form. Based on linear state-space theory, the displacement and acceleration transfer functions $\mathbf{G_d}$ and $\mathbf{G_a}$ are given as

$$\mathbf{G_d}(s;\mathbf{p}) = \mathbf{E}(s\mathbf{I} - \mathbf{A}(\mathbf{p}))^{-1}\mathbf{B} \tag{7}$$

$$\mathbf{G_a}(s;\mathbf{p}) = \mathbf{E}[\mathbf{A}(s\mathbf{I} - \mathbf{A}(\mathbf{p}))^{-1} + \mathbf{I}]\mathbf{B} \tag{8}$$

where

$$\mathbf{A}(\mathbf{p}) = \begin{bmatrix} \mathbf{0} & \mathbf{I} \\ -\mathbf{M}(\mathbf{p})^{-1}\mathbf{K}(\mathbf{p}) & -\mathbf{M}(\mathbf{p})^{-1}\mathbf{C}(\mathbf{p}) \end{bmatrix}, \quad \mathbf{B} = \begin{bmatrix} \mathbf{0} \\ -\mathbf{M}(\mathbf{p})^{-1}\mathbf{M_l} \end{bmatrix} \tag{9}$$

where $\mathbf{p} = [f_1, f_t, \beta_t, \zeta_t]$ denotes the design parameters of TMDI-TIBD; $\mathbf{I}$ and $\mathbf{0}$ are the identity and zero matrices, respectively; the vector $\mathbf{E}$ describes the output in state space, and it is taken to be $[1, 0, 0, 0, 0, 0]$ for the displacement transfer function and $[0, 0, 0, 1, 0, 0]$ for the acceleration transfer function.

3. Optimal design of TMDI-TIBD in SDOF structures

As an extension of the TMD, the optimal parameters of a TMDI can be directly found by modifying the tuned mass ratio to $\mu + \beta_1$ for a structure subjected to a harmonic load. Yet, there are hardly any explicit expressions for the optimal parameters of TMDI when the structure is subjected to harmonic excitation. Therefore, in this section, our focus is on designing the optimal parameters of TMDI-TIBD using the fixed-point theory when the primary structure is subjected to harmonic excitation. Under harmonic loading, the optimal parameters of TMDI-TIBD can be derived directly by redefining the tuned mass ratio of IDVA [20] as $\mu + \beta_1$.

3.1. Minimizing displacement transfer function via fixed-point theory

According to fixed-point theory, two individual equations are generated when the damping ratio of the dampers converges to 0 and infinity, respectively:

$$|H_d|_{\zeta_t \to 0} = \sqrt{\frac{A^2}{C^2}}, \quad |H_d|_{\zeta_t \to \infty} = \sqrt{\frac{B^2}{D^2}}. \tag{10}$$

Subsequently, based on the core text of fixed-point theory, there are always four points with equal amplitude regardless of the damping ratio of the tuned dampers, which can be observed in Fig. 2(a) with the optimal β_t, f_1, f_t derived by the next process,

$$\frac{A}{C} = \pm\frac{B}{D}. \tag{11}$$

The positive term can be ignored because it only produces three trivial solutions $\beta_t = 0, f_1 = 0, f_t = 0$, and Eq. (11) can be rearranged as

$$a\Gamma^4 + b\Gamma^3 + c\Gamma^2 + d\Gamma + e = 0 \tag{12}$$

where $\Gamma = \gamma^2$ and the expressions of a, b, c, d, e are listed in Appendix B. Based on Vieta's theorem for quartic equations, the sum and product of the roots can be derived from the coefficients of this equation:

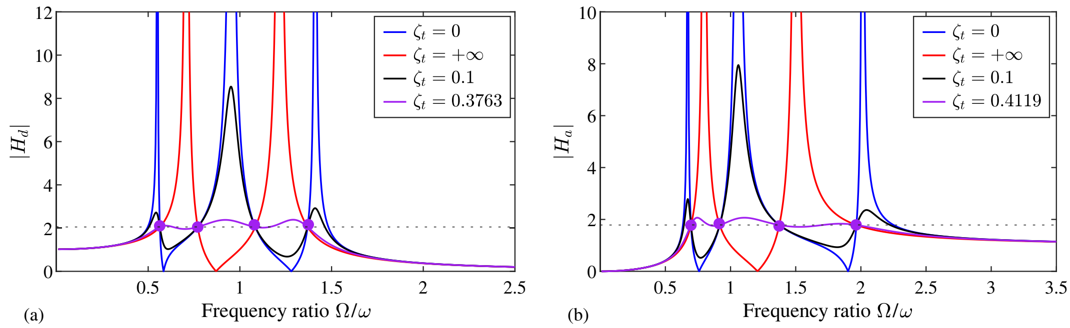

Fig. 2. Invariant point of (a) displacement frequency response and (b) acceleration frequency response curves of the TMDI-TVMD controlled strategy at optimal β_t, f_1, f_t. ($\mu = 0.02, \beta_1 = 0.3$).

$$\begin{aligned}
&\sum_{i=1}^{4} \Gamma_i = -\frac{b}{a},\\
&\sum_{i,j=1}^{4} \Gamma_i \Gamma_j = \frac{c}{a} \quad (i<j),\\
&\sum_{i,j,k=1}^{4} \Gamma_i \Gamma_j \Gamma_k = -\frac{d}{a} \quad (i<j<k),\\
&\prod_{i=1}^{4} \Gamma_i = \frac{e}{a}.
\end{aligned} \tag{13}$$

Additionally, a quartic equation with Γ^2 as its variable and containing displacement amplitude H_d is produced by considering $\left(H_d\right)^2_{\zeta_t \to \infty} = B^2/D^2$:

$$a'\Gamma^4 + b'\Gamma^3 + c'\Gamma^2 + d'\Gamma + e' = 0 \tag{14}$$

where the expressions of a', b', c', d' are described in Appendix B. Four similar equations are formed by Vieta's theory. Consequently, the following four equations emerge by combining Eqs. (12)–(14):

$$\frac{b}{a} = \frac{b'}{a'}, \quad \frac{c}{a} = \frac{c'}{a'}, \quad \frac{d}{a} = \frac{d'}{a'}, \quad \frac{e}{a} = \frac{e'}{a'}. \tag{15}$$

Finally, the optimal design parameters β_t, f_1, f_t of TMDI-TIBD are derived by solving these four high-order equations with β_t, f_1, f_t, H_d as variables. For the TMDI-TVMD case, the optimal solutions are:

$$\begin{aligned}
\beta_t^d &= \frac{2(1+\mu)\left(\mu+\beta_1\right)}{\left((1+\mu)^2+\beta_1(\mu+2)\right)^2},\\
f_1^d &= \sqrt{\frac{1-\mu\left(\mu+\beta_1\right)}{(1+\mu)\left((1+\mu)^3+\beta_1^3(\mu+2)+\beta_1\left(2\mu^2+5\mu+3\right)\right)}},\\
f_t^d &= \frac{1+(\mu+2)\left(\mu+\beta_1\right)}{\sqrt{1-\mu\left(\mu+\beta_1\right)}},\\
\left|H^d\right| &= \sqrt{\frac{(1+\mu)\left(1+\mu+\beta_1\right)}{\mu+\beta_1}}.
\end{aligned} \tag{16}$$

For the TMDI-TID case, the optimal solutions are:

$$\begin{aligned}
\beta_t^d &= \frac{-1+\beta_1+\mu+2\mu\left(\beta_1+\mu\right)+\kappa_1}{\left(1+\beta_1+\mu\right)\left(2-\mu\left(-1+\beta_1+\mu\right)\right)},\\
f_1^d &= \sqrt{\frac{1-\left(\beta_1+\mu\right)(2\mu+1)+\kappa_1}{2(\mu+1)\left(1+\beta_1+\mu\right)^2}},\\
f_t^d &= \sqrt{\frac{-\left(1+\beta_1+\mu\right)\kappa_2}{2\left(\mu+\mu^2+\beta_1(2+\mu)\right)^2}},\\
\left|H^d\right| &= \sqrt{\frac{(1+\mu)\left(1+\beta_1+\mu+\kappa_1\right)\kappa_4}{2\left(\beta_1+\mu\right)\left(2\mu(1+\mu)+\beta_1(2+\mu)\right)\kappa_3}},
\end{aligned} \tag{17}$$

where

$$\begin{aligned}
\kappa_1 &= \sqrt{\beta_1^2+2\beta_1(\mu+1)(2\mu+3)+(\mu+1)^2(4\mu+1)},\\
\kappa_2 &= \left(\mu\beta_1^2+(1+\mu)\left(2\left(-1+\kappa_1\right)+\mu\left(-7-5\mu+\kappa_1\right)\right)\right.\\
&\quad \left.+\beta_1\left(-6+\mu\left(-10-4\mu+\kappa_1\right)\right)\right),\\
\kappa_3 &= \mu^2(\mu-6)(1+\mu)^3+\mu\beta_1^3(2+\mu(\mu+4))\\
&\quad +\mu\beta_1(1+\mu)^2(-10+\mu(3\mu-8))+\beta_1^2(1+\mu)(-4+\mu(2+\mu)(-4+3\mu)),\\
\kappa_4 &= 2\mu^3(-6+\mu)(1+\mu)^4+\beta_1\mu^2(-4+\mu)(8+7\mu)(1+\mu)^3\\
&\quad +\beta_1^3(1+\mu)\left(-8-20\mu+16\mu^3+5\mu^4\right)+\mu\beta_1^4(2+\mu)(2+\mu(4+\mu))\\
&\quad +\mu\beta_1^2(1+\mu)^2(-28+\mu(-42+\mu(2+9\mu))).
\end{aligned} \tag{18}$$

Notably, $|H^d|$ denotes the equal amplitude of four fixed points (shown as a gray dotted line in Fig. 2), and the dimensionless amplitude $|H_d|$ is equal to $1+\mu$ at point $\gamma = 0$ for the controlled structure subjected to ground acceleration input [46,47].

3.2. Minimizing acceleration transfer function via fixed-point theory

The expressions of acceleration amplitude at four fixed points are generated without considering the variation in the damping ratio of the dampers,

$$|H_a|_{\zeta_t \to 0} = \sqrt{\frac{\gamma^4 A^2}{C^2}}, \quad |H_a|_{\zeta_t \to \infty} = \sqrt{\frac{\gamma^4 B^2}{D^2}}. \tag{19}$$

By imitating the above design procedures for the goal of minimizing the relative displacement, the optimal tuned parameters of TMDI-TIBD to minimize the acceleration amplitude can be directly derived.

For the TMDI-TVMD case, the optimal solutions are:

$$\begin{aligned}
\beta_t^a &= \frac{2\left(\mu+\beta_1\right)\left(1-\beta_1\right)}{\left(1+2\mu+\beta_1\right)^2},\\
f_1^a &= \sqrt{\frac{1}{1+2\mu+\beta_1}},\\
f_t^a &= \frac{1+2\mu+\beta_1}{\sqrt{1-2\beta_1+\beta_1^2}},\\
|H^a| &= \frac{\sqrt{(1+\mu)\left(\mu+\beta_1\right)}}{\mu+\beta_1}.
\end{aligned} \tag{20}$$

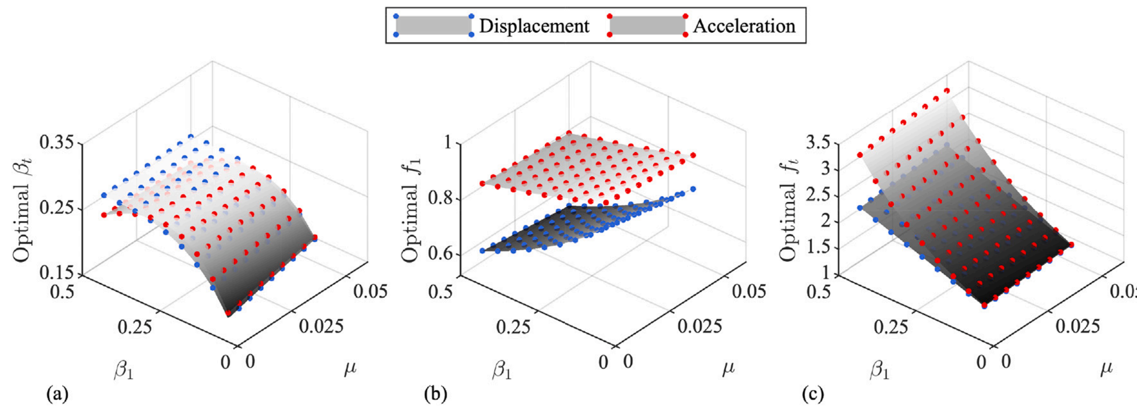

Fig. 3. Optimal parameters of TMDI-TVMD: (a) inertance-mass ratio of TIBD; (b) frequency ratio of tuned mass; (c) frequency ratio of TIBD. ($\zeta = 0$).

For the TMDI-TID case, the optimal solutions are:

$$\beta_t^a = \frac{-1+\beta_1+\mu\beta_1+\mu^2+\kappa_1}{2(1+\mu)\left(1+\mu+\beta_1\right)},$$
$$f_1^a = \sqrt{\frac{1+\mu(\mu+2)+\beta_1(\mu+3)+\kappa_1}{2(1+\mu)\left(1+\mu+\beta_1\right)^2}},$$
$$f_t^a = \sqrt{\frac{1+3\beta_1(1+\mu)+\mu(3\mu+4)-\kappa_1}{4\mu\left(\beta_1+\mu\right)}},$$
$$|H^a| = \sqrt{\frac{(1+\mu)\left(1+\mu(2+\mu)+\beta_1(3+\mu)+\kappa_1\right)}{2\left(\beta_1+\mu\right)\left(1+\beta_1+\mu\right)^2}},$$
$$\kappa_1 = \sqrt{(1+\mu)\left(\beta_1^2(\mu+9)+(1+\mu)(1+\mu(\mu+6))+2\beta_1(3+\mu(\mu+8))\right)}. \tag{21}$$

Fig. 3 shows the relationships between the optimal design parameters of TMDI-TVMD and the tuned mass ratio μ as well as the inertance-mass ratio β_1. The optimal inertance-mass ratio of the tuned inerter-based damper β_t (derived from the displacement frequency-response function) exhibits an exponential growth pattern with increasing β_1, while it increases progressively with a larger μ. However, for controlling the acceleration response, $\beta_1 = 0.3$ is a noticeable point, as the optimal β_t has a nonlinear increment trend initially but changes the variation pattern if it crosses the critical point. Furthermore, $\beta_1 = 0.3$ has an identical effect on the relationship between the optimal β_t and the tuned mass ratio μ. Additionally, for controlling the displacement and acceleration responses, the optimal frequency ratio of the tuned mass f_1 presents a nearly linear progression with increasing μ and β_1, while the optimal frequency ratio of tuned inerter-based dampers f_t has the opposite variation pattern under the same condition. Furthermore, the optimal f_1 obtained by minimizing the displacement amplitude is more sensitive than that based on the acceleration amplitude, whereas the opposite phenomenon is observed for the optimal f_t.

3.3. Simplification of optimal damping ratio

The optimal damping ratio of an absorber is defined by $\partial H/\partial\gamma = 0$, which can produce a relationship between the damping ratio and tuned mass ratio, as described by Den Hartog. The frequency-response function can reach its maximum at two fixed points for TMD; but the identical conclusion cannot be extended to TMDI-TIBD, as demonstrated in Fig. 2. Under the condition of $\mu = 0.02$ and $\beta_1 = 0.3$, the optimal frequency-response curves from numerical ζ_t and analytical β_t, f_1, f_t are drawn as purple lines, and the amplitude does not occur at the fixed points (purple circle). Hence, the conventional fixed-point theory is not appropriate for the TMDI-TIBD absorber. Although Barredo et al. [20] introduced Krenk's method to find the optimal damping ratio for double-tuned inerter-based dampers (which is a special form of TMDI-TIBD with $\beta_1 = 0$), the analytical solution is extremely complicated. Therefore, a data-fitting method is employed to establish the expression of the optimal damping ratio to facilitate the use of TMDI-TIBD.

First, the optimal solution of ζ_t is determined after the numerical optimization of TMDI-TIBD over μ and β_1 within the range of 0.01–0.05 and 0.1–0.5, while other design parameters are figured out by the above analytical solutions. The mathematical operation can be listed as

$$\zeta_t^{d,a} = \underset{\zeta_t}{\operatorname{argmin}}\left\{\|\mathbf{G}(s;\zeta_t)\|_\infty\right\}. \quad \text{s.t.} \quad \beta_t = \beta_t^{d,a}, f_1 = f_1^{d,a}, f_t = f_t^{d,a}. \tag{22}$$

Afterward, the curve-fitting toolbox embedded in MATLAB is employed to generate the fitting formula of the optimal damping ratio of TMDI-TIBD. For the TMDI-TVMD and TMDI-TID cases, the optimal solutions of ζ_t are given as:

$$\zeta_{t,TMDI-TVMD}^d = \sqrt{\frac{0.5039\beta_1+0.3851\beta_1^2+0.4897\mu+0.1862\mu^2+0.5181\mu\beta_1}{0.6427+2.0321\beta_1+1.335\beta_1^2+1.2993\mu+1.6836\mu^2+1.0206\mu\beta_1}},$$
$$\zeta_{t,TMDI-TID}^d = \sqrt{\frac{0.3161\beta_1+0.3151\beta_1^2+0.3414\mu+0.2829\mu^2+0.6298\mu\beta_1}{0.4052+1.6865\beta_1+1.0479\beta_1^2+1.372\mu+0.3939\mu^2-0.265\mu\beta_1}},$$
$$\zeta_{t,TMDI-TVMD}^a = \sqrt{\frac{0.4165\beta_1+0.4162\beta_1^2+0.4303\mu-0.1322\mu^2+0.2974\mu\beta_1}{0.53+1.2631\beta_1+0.9613\beta_1^2+0.9237\mu+0.0553\mu^2+0.6547\mu\beta_1}},$$
$$\zeta_{t,TMDI-TID}^a = \sqrt{\frac{0.4124\beta_1+0.214\beta_1^2+0.4325\mu-0.0054\mu^2+0.3573\mu\beta_1}{0.551+2.2164\beta_1+0.9164\beta_1^2+2.3134\mu-0.6042\mu^2+0.829\mu\beta_1}}. \tag{23}$$

Fig. 4 compares the numerical solution and the fitting formula with the goal of minimizing displacement and acceleration frequency-response functions of the TMDI-TVMD control strategy at $\zeta = 0$, and the results are fairly compatible. Moreover, the optimal damping ratio of TMDI-TVMD has a positive correlation with both the tuned mass ratio μ and the inertance-mass ratio β_1, and it has a wider scope of variation for optimizing the acceleration response.

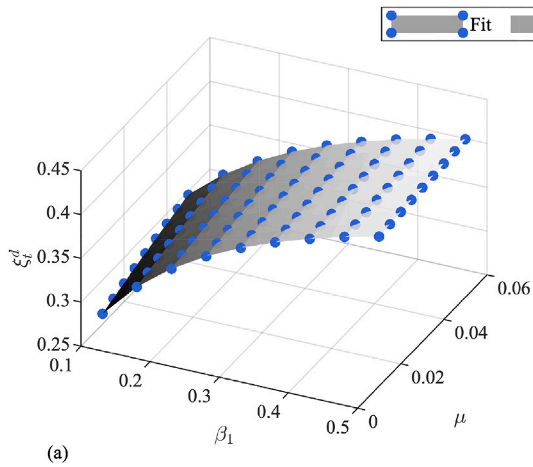

Fig. 4. Comparison for the optimal damping ratio of TMDI-TVMD aimed at minimizing the (a) displacement and (b) acceleration objectives between numerical optimization and the fitting formula.

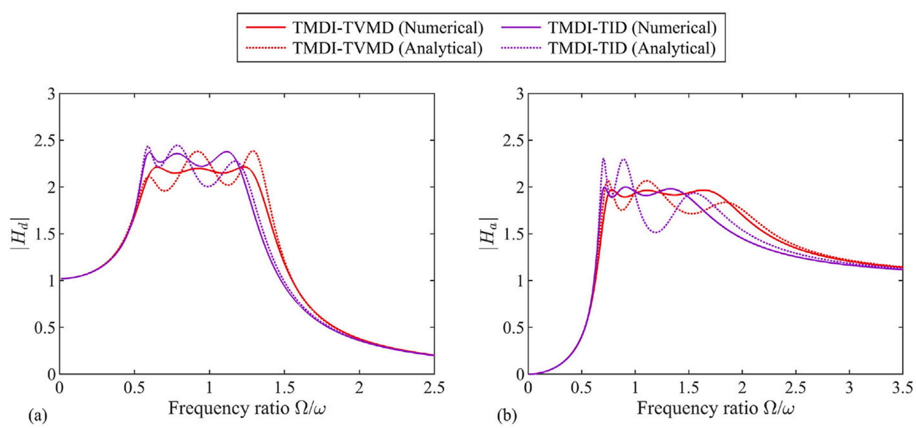

Fig. 5. (a) Displacement and (b) acceleration frequency response curves of undamped structure controlled by optimal TMDI-TIBD with analytical and numerical solutions. ($\mu = 0.02, \beta_1 = 0.3$).

3.4. Comparison with numerical optimization

Numerical optimization can be used to obtain the optimal parameters of TMDI-TIBD for controlling either an undamped or damped structure. In particular, the numerical solutions of TMDI-TIBD are derived by minimizing the H_∞ norm of its transfer functions,

$$\mathbf{p}^{opt} = \underset{\mathbf{p}}{\operatorname{argmin}} \left\{ \|\mathbf{G}(s;\mathbf{p})\|_\infty \right\}. \tag{24}$$

First, Fig. 5 compares the frequency-response curves of an undamped structure equipped with the optimally designed TMDI-TIBD, derived from numerical and analytical solutions. Both solutions of TMDI-TIBD (minimized displacement and minimized acceleration) are presented. Fig. 5 shows that there are certain discrepancies between the numerical and analytical solutions. These errors, introduced by the fixed-point method, appear to be unavoidable and are independent of the structural damping ratio. The similar phenomenon can be found in [20,48]. Therefore, the fitted closed-form solution of optimal damping ratio ζ_t derives from the undamped structure. To further investigate the applicability of closed-form solutions derived by the undamped structure in the damped structure, the deviations of displacement and acceleration amplitudes for numerical and analytical solutions with varying structural damping ratios ζ in 0–0.05 are depicted in Fig. 6. It can be seen that structural damping and inertance have certain influences on the accuracy of analytical solutions, but the analytical solutions obtained from the undamped structure show an acceptable error when applied to lightly damped structures, maintaining a within 5 % average deviation.

4. Performance analysis of TMDI-TIBD in SDOF structures

In this section, the control effect, stroke of the tuned mass block, and the sensitivity of control performance to design parameters are analyzed. Noticeably, all the parameters of control strategies in the comparison are on the basis of numerical solutions to make the analysis more reasonable and dislodge the error of closed-form solutions. In comparison with TMDI, the tuned mass ratios of TMDI-TIBD and TMDI are equal. While compared with TMD, except for the above condition, a TMD whose tuned mass ratio equals the sum of the tuned mass and inertance-mass ratios used by TMDI-TIBD is also taken into consideration.

4.1. Optimal performance of TMDI-TIBD

To show the optimal performance of vibration suppression by TMDI-TIBD, Fig. 7 plots the frequency responses for undamped structures equipped with an optimally designed TMDI-TIBD based on H_∞ norm. It is observed that the larger the inertance and tuned mass of TMDI-TIBD, the better the control performance and the stronger robustness that can be achieved. The broadening of the control bandwidth dramatically decreases the exposure of detuning in the dampers, especially for TMDI-TVMD in suppressing the acceleration resonant response. Note that TMDI-TIBD also shows effective control over the resonant response

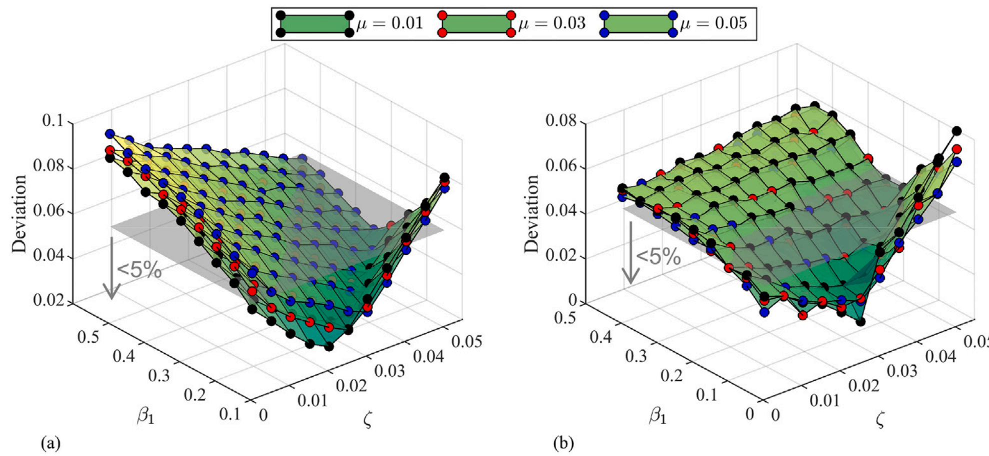

Fig. 6. Deviation between numerical and closed-form solutions of TMDI-TVMD aimed at minimizing the (a) displacement and (b) acceleration amplitudes.

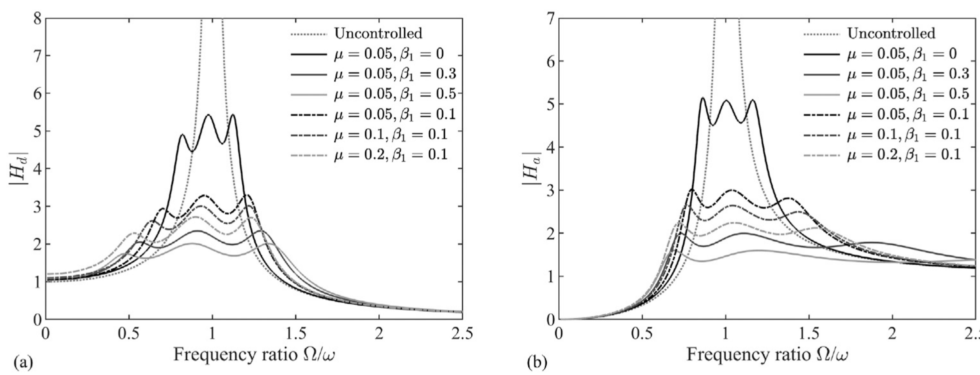

Fig. 7. Comparison of (a) displacement and (b) acceleration frequency response curves of the TMDI-TVMD controlled structure under closed-form solutions.

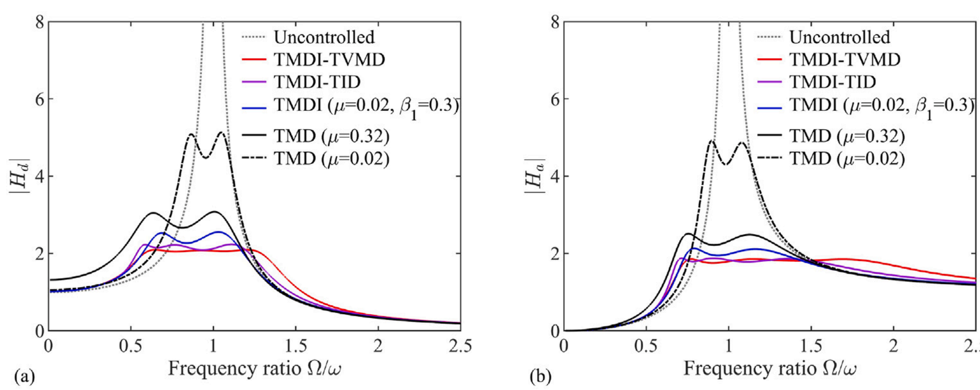

Fig. 8. Comparison of structural response amplitudes between TMDI-TIBD, TMD, and TMDI under optimal design to minimize (a) displacement and (b) acceleration amplitudes. ($\zeta = 0.02$).

when $\beta_1 = 0$, which represents a special case illustrated in Fig. 1. In addition, the effect of increasing β_1 is similar to that of increasing μ, which precisely demonstrates the mass-amplification effect of the inerter in TMDI-TIBD.

4.2. Comparison with TMDI and TMD

To investigate the difference between TMDI-TIBD, TMDI, and TMD, the displacement and acceleration frequency-response curves of an SDOF structure controlled by these three strategies are depicted in Fig. 8, where the mass ratio μ and inertance-mass ratio β_1 of TMDI-TIBD are identical to those used in TMDI. It can be observed that, at the same tuned mass ratio $\mu = 0.02$, TMDI-TIBD shows the best control performance and robustness for structural responses. When the sum of μ and β_1 in TMDI-TIBD equals the tuned mass ratio $\mu = 0.32$ in TMD, TMDI-TIBD still exhibits better control performance and stronger robustness. Fig. 9 further evaluates the amplitude ratios of the peak displacement and acceleration of TMDI-TVMD relative to TMD and TMDI, with the tuned mass of TMD, TMDI, and TMDI-TVMD kept equal. As can be seen, the control performance of TMDI-TVMD can be greatly enhanced by increasing β_1, compared with a conventional TMD. In addition, when $\beta_1 = 0$, the improvement arises from the introduction of TIBD. Compared with

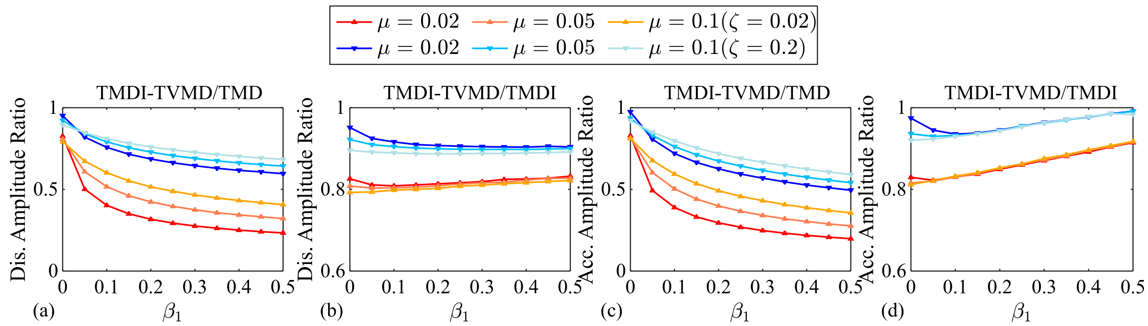

Fig. 9. (a) and (b) Displacement and (c) and (d) acceleration amplitude ratios of TMDI-TVMD to (a) and (c) TMD and (b) and (d) TMDI.

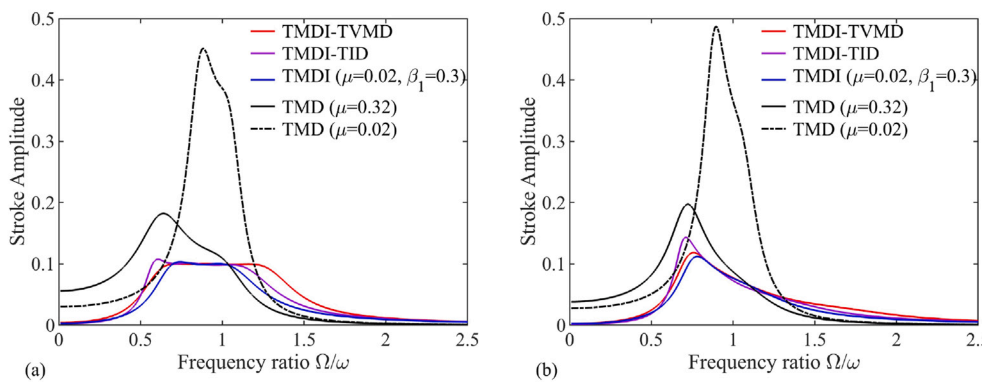

Fig. 10. Comparison of tuned mass strokes between TMDI-TIBD, TMD, and TMDI under optimal design to minimize (a) displacement and (b) acceleration amplitudes. (ζ = 0.02).

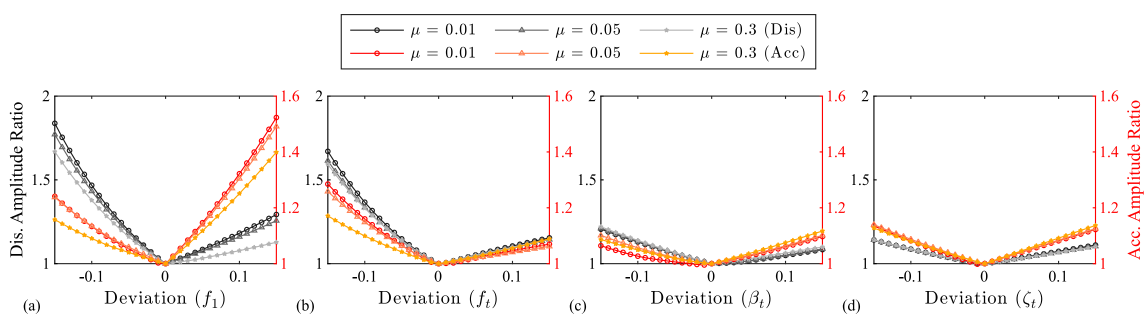

Fig. 11. Amplitude amplification ratio of the TMDI-TVMD controlled system with variation in (a) tuned frequency ratio f_1, (b) tuned frequency ratio f_t, (c) inertance-mass ratio β_t, and (d) damping ratio ζ_t.

TMDI, the enhancement offered by TMDI-TIBD is dominated by the introduced TIBD, as increasing β_1 is ineffective for further improvement. Furthermore, TMDI-TIBD provides a significant enhancement in control performance for structures with a smaller damping ratio.

4.3. Analysis of tuned mass stroke

Although an optimally designed TMDI-TIBD can enhance the structural vibration control performance compared with TMDI and TMD, the stroke of the tuned mass is also noticeable. Its tuned mass strokes corresponding to Fig. 8 are compared in Fig. 10, where the tuned mass and inertance-mass ratios of TMDI-TIBD have the same values as those of TMDI. The tuned mass stroke of a classical TMD is greatly reduced when a 30 % tuned mass ratio is used. Meanwhile, for TMDI-TIBD and TMDI, increasing a 30 % inertance-mass ratio is more effective. When their tuned mass ratio is the same, the tuned mass stroke of TMDI-TIBD is noticeably smaller than that of the TMD and is close to or slightly greater than that of the TMDI.

4.4. Sensitivity analysis of TMDI-TIBD

To show the influence of any variation in the optimal parameters of TMDI-TIBD on control performance, we analyze the structural responses by shifting design parameters from their optimal values. Fig. 11 plots the displacement and acceleration amplitude ratios of the TMDI-TVMD-controlled structure before and after a 15 % deviation of the four optimally designed parameters.

From a horizontal view, the control performance of TMDI-TVMD is more sensitive to the two tuned-frequency parameters f_1 and f_t than to the inertance-mass ratio β_t and the damping ratio ζ_t. For the displacement- and acceleration-based optimal-design solutions, increasing or decreasing the design-parameter values can have different influences on the structural response. For instance, the acceleration-based optimal-design TMDI-TVMD shows stronger resistance to stiffness degradation of k_1. To enhance the robustness of TMDI-TVMD, increasing the tuned-mass ratio μ or the inertance-mass ratio β_1 is beneficial. To further investigate the control robustness of TMDI-TVMD compared with

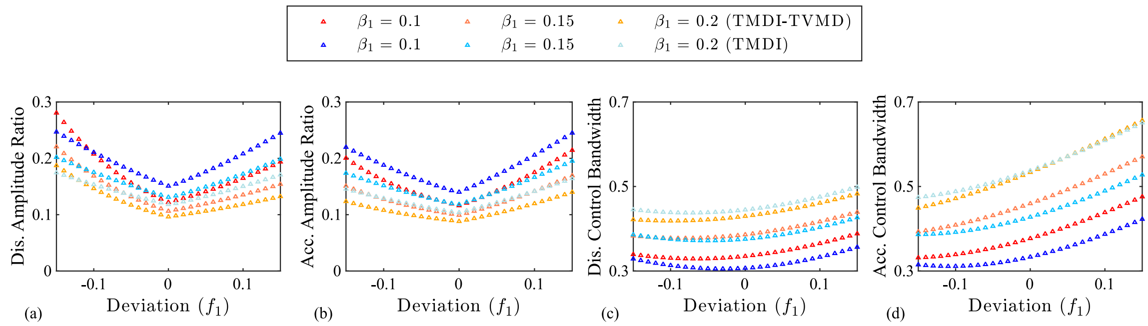

Fig. 12. Amplitude ratios and control bandwidth of TMDI-TVMD and TMDI relative to uncontrolled structures. (a) displacement amplitude ratio; (b) acceleration amplitude ratio; (c) control bandwidth of displacement; and (d) control bandwidth of acceleration. ($\mu = 0.02, \zeta = 0.02$).

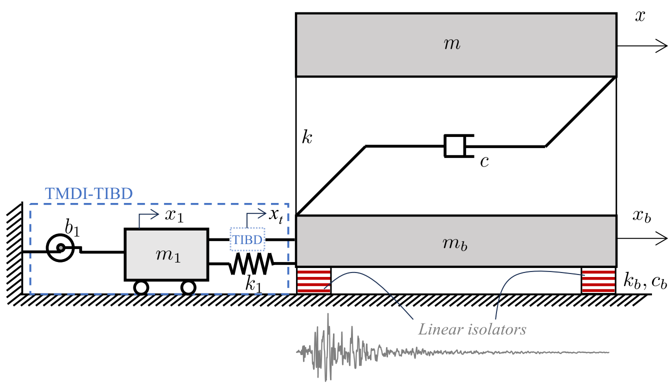

Fig. 13. Analysis model of a TMDI-TIBD-enhanced base isolation system.

TMDI, the response-amplitude ratios and control bandwidth of TMDI-TVMD- and TMDI-controlled structures at the same tuned-mass ratio $\mu = 0.02$ are shown in Fig. 12. It can be seen that TMDI-TVMD exhibits stronger robustness in reducing peak response and maintaining a wider control bandwidth.

5. Performance of TMDI-TIBD in a base-isolated structure

The mass-amplification effect of the inerter can be utilized most adequately when the inerter is connected to the ground, so the TMDI has been proposed to control the excessive displacement of the BIS [27]. In this section, the TMDI-TIBD is introduced into the BIS. The schematic of this BIS combined with TMDI-TIBD is illustrated in Fig. 13, where one side of the TMDI-TIBD is connected to the isolation floor and the other is connected to the ground. Additionally, this section focuses on analyzing a BIS enhanced by TMDI-TVMD, as it presents better control performance than TMDI-TID in the previous analysis.

5.1. Equation of motion

The governing equation of motion of an SDOF structure equipped with the enhanced BIS is given by Eq. (25):

$$\hat{\mathbf{M}}\ddot{\mathbf{x}} + \hat{\mathbf{C}}\dot{\mathbf{x}} + \hat{\mathbf{K}}\mathbf{x} = -\tau \ddot{x}_g. \tag{25}$$

$$\hat{\mathbf{M}} = \begin{bmatrix} m & m & 0 & 0 \\ m & m+m_b & 0 & 0 \\ 0 & 0 & m_1+b_1+b_t & -b_t \\ 0 & 0 & -b_t & b_t \end{bmatrix}, \quad \hat{\mathbf{C}} = \begin{bmatrix} c & 0 & 0 & 0 \\ 0 & c_b & 0 & 0 \\ 0 & 0 & c_t & -c_t \\ 0 & 0 & -c_t & c_t \end{bmatrix},$$
$$\hat{\mathbf{K}} = \begin{bmatrix} k & 0 & 0 & 0 \\ 0 & k_b+k_1+k_t & -k_1 & -k_t \\ 0 & -k_1 & k_1 & 0 \\ 0 & -k_t & 0 & k_t \end{bmatrix}; \tag{26}$$

where $\mathbf{x} = [x_{sr}, x_b, x_1, x_t]^{\mathrm{T}}$ is the displacement vector, with $x_{sr} = x - x_b$ denoting the relative displacement of the superstructure. The vector $\tau = [m, m+m_b, m_1, 0]^{\mathrm{T}}$ represents the load, where m, m_b, and m_1 are the masses of the superstructure, isolation layer, and tuned mass of TMDI-TIBD. Meanwhile, k_b and c_b are the stiffness and damping coefficients of the isolation layer. For the BIS, the following parameters describe its characteristics:

$$T_b = \frac{2\pi}{\omega_b}, \quad \zeta_b = \frac{c_b}{2(m_b+m)\omega_b}, \quad \omega_b = \sqrt{\frac{k_b}{m_b+m}}, \quad \mu_b = \frac{m_b}{m}, \quad f_b = \frac{\omega_b}{\omega}; \tag{27}$$

where T_b denotes the fundamental period of the BIS, which is fixed at 3 s to match common engineering-design practice.

5.2. Optimal design of TMDI-TIBD

In a BIS, the superstructure's response is governed primarily by translational motion. Consequently, the BIS can be idealized as an SDOF system with a large effective mass and a long natural period. Under this idealization, applying the closed-form design formulas for the TMDI-TIBD is appropriate. Accordingly, the tuned-mass ratio μ, the inertance-mass ratio β_1, and the frequency ratio f_1 are redefined by the specific characteristics of the BIS as follows:

$$\mu = \frac{m_1}{m+m_b}, \quad \beta_1 = \frac{b_1}{m+m_b}, \quad f_1 = \frac{\omega_1}{\omega_b}. \tag{28}$$

Subsequently, the optimal parameters of TMDI-TIBD in a BIS can be designed by:

$$b_t = (m_1+b_1)\beta_t, \quad k_1 = (m_1+b_1)f_1^2\omega_b^2, \quad k_t = b_t(\omega_b f_1 f_t)^2, \quad c_t = 2\zeta_t\sqrt{b_t k_t}; \tag{29}$$

where ω_b represents the predominant frequency of the BIS. Given specified values of μ and β_1, the optimal β_t, f_1, f_t, and ζ_t are obtained, and the damper parameters are determined from Eqs. (28) and (29). As in the SDOF case, two performance metrics: structural displacement and acceleration, serve as the optimization objectives:

$$\mathrm{OF}_1 = |H_d|, \quad \mathrm{OF}_2 = |H_a|. \tag{30}$$

Closed-form solutions for both the TMD and the TMDI under base excitation, with the objective of minimizing displacement amplitude, have been reported previously [46,47]. Warburton [46] also derived expressions for a TMD to minimize acceleration amplitude. Comparable closed-form solutions for the TMDI, however, are not yet available, so explicit formulas cannot be used in the present work. Accordingly, we rely on implicit formulations to obtain the optimal TMDI parameters.

Based on these design strategies, Fig. 14(a) and (c) reports the displacement and acceleration amplitude ratios between the TMDI-TVMD-enhanced BIS and the conventional BIS, while Fig. 14(b) and (d) presents the displacement and acceleration amplitude ratios between

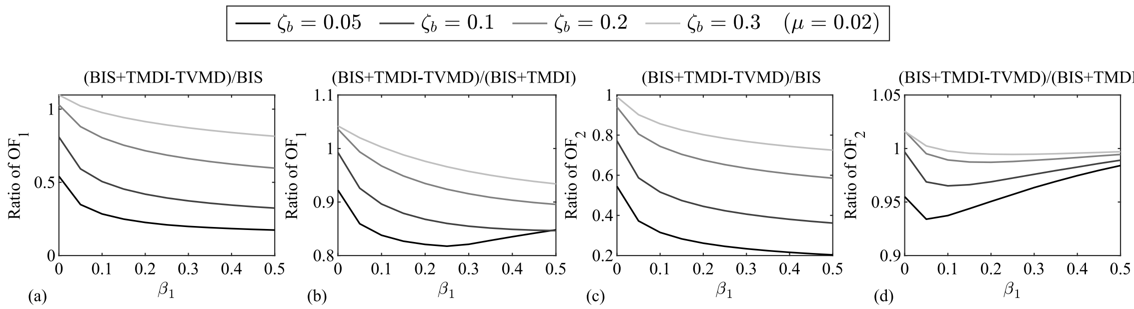

Fig. 14. Performance ratio of the TMDI-TVMD-enhanced BIS compared to (a) and (c) a conventional BIS and (b) and (d) a TMDI-enhanced BIS at the same tuned mass ratio. ($\mu_b = 0.2$, $f_b = 0.1$, $T_b = 3$ s, $\omega = 2\pi/0.3$ rad/s, $\xi = 0.02$).

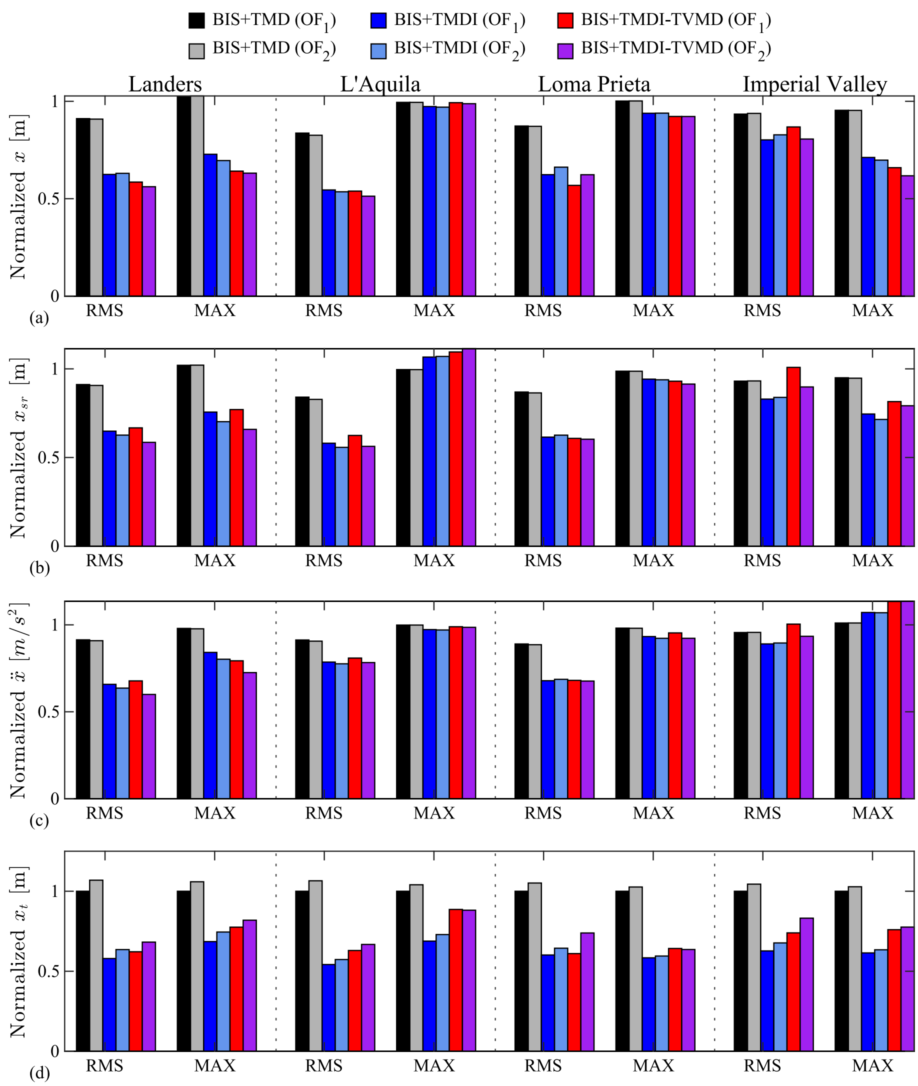

Fig. 15. Comparison of root mean square (RMS) and maximum (MAX) responses of (a) structural displacement, (b) relative displacement of the superstructure, (c) structural absolute acceleration, and (d) tuned mass stroke of the BIS with different strategies excited by four ground motions. ($\mu = 0.02, \beta_1 = 0.1$).

the TMDI-TVMD-enhanced BIS and the TMDI-enhanced BIS. Clearly, the improvement of a TMDI-TVMD-enhanced BIS compared to a conventional BIS is more pronounced in a low-damping BIS, similar to the TMDI-enhanced BIS [27]. Compared with the TMDI-enhanced BIS, a TMDI-TVMD-enhanced BIS shows certain improvements, which are also more obvious for a low-damping BIS with smaller β_1 , especially for the displacement objective.

5.3. Seismic analysis

To evaluate the seismic performance of a TMDI-TVMD-enhanced BIS, four representative ground motions, Landers, L'Aquila, Loma Prieta, and Imperial Valley, selected from the Center for Engineering Strong Motion Data website (http://strongmotioncenter.org/) are used. Detailed information on the four ground motions can be found in Fig. C1 (Appendix C).

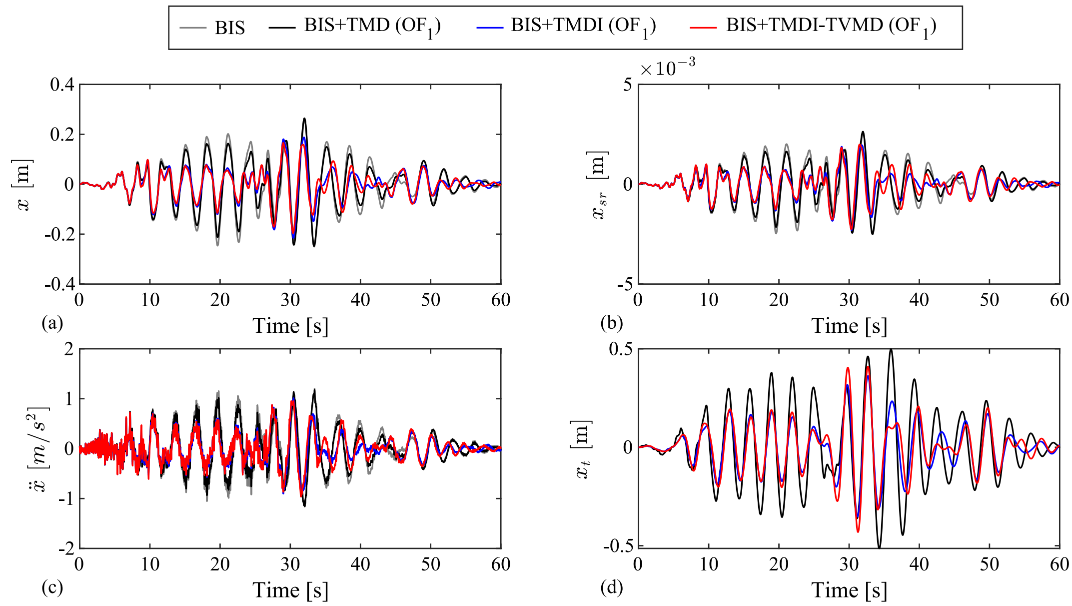

Fig. 16. Comparison of time-history curves of (a) structural displacement, (b) relative displacement of the superstructure, (c) structural absolute acceleration, and (d) tuned mass stroke of the BIS with different strategies excited by the Landers record. ($\mu = 0.02, \beta_1 = 0.1$).

Here, the structural parameters of the BIS are $\mu_b = 0.2$, $\zeta_b = 0.05$, $f_b = 0.1$, representing a multistory low-damping base-isolated building. For the TMDI-TVMD and TMDI strategies, $\mu = 0.02, \beta_1 = 0.10$ are chosen. For the TMD strategy, $\mu = 0.02+0.10 = 0.12$ is used to maintain a similar total mass ratio to the TMDI-TVMD and TMDI strategies due to the mass amplification effect of the inerter.

We compare the time-history responses of the structural displacement and absolute acceleration, the relative displacement of the superstructure, and the tuned-mass stroke for the three strategies against the conventional BIS. The maximum and variance responses of the enhanced BIS under the three strategies across four seismic excitations are presented in Fig. 15, and the time-history response curves excited by the Landers record are shown in Fig. 16. Note that the response amplitudes in Fig. 15 are normalized to the response of the conventional BIS to highlight the performance of the analyzed control strategies.

It can be seen that the TMDI-TIBD shows an obvious improvement over the TMD strategy in controlling the structural top displacement x, the relative displacement of the superstructure x_{sr}, and the tuned-mass stroke x_t, since the TMD can barely control the seismic responses of the BIS and has an excessive stroke. Compared to the TMDI strategy, the TMDI-TVMD strategy shows a slight enhancement in control at the cost of slightly amplifying the tuned-mass stroke. The improvement of TMDI-TIBD is not extremely prominent, which may be because the frequency characteristic of the seismic excitation does not induce significant resonant responses in the BIS, unlike the conclusion drawn from harmonic excitation. In other words, the advantage of TMDI-TVMD in a BIS is largely dominated by the mass-amplification effect of the inerter.

6. Conclusions

To enhance the control performance and robustness of the conventional TMD, this paper proposes an enhanced TMDI using the tuned inerter-based damper (TMDI-TIBD). First, the dynamic equations and transfer functions of TMDI-TIBD are established. Second, closed-form solutions for the optimal design parameters of TMDI-TIBD are obtained using the fixed-point theory to minimize the displacement and acceleration responses. Third, the performance of TMDI-TIBD is compared with that of TMD and TMDI, and is comprehensively evaluated in terms of structural control performance, tuned mass stroke, and parameter sensitivity. Finally, TMDI-TIBD is introduced into the BIS to improve its vibration-isolation performance or reduce its tuned-mass demand, in comparison to a conventional TMD strategy. The main conclusions of this article are as follows.

1. Closed-form solutions for the optimal design parameters of TMDI-TIBD are derived via fixed-point theory to minimize the structural displacement and acceleration transfer functions of undamped structures. In particular, the optimal damping ratios of TMDI-TIBD are simplified using the proposed fitted formulas to avoid complex theoretical expressions. These closed-form solutions are accurate enough, with an average deviation within 5 % when compared with the numerical optimization results of undamped and damped structures. Sensitivity analysis of the optimal parameters of TMDI-TVMD shows that tuning stiffnesses k_1 and k_t dominate changes in its optimal performance; the acceleration-based optimal-design parameters exhibit an advantage under stiffness degradation.
2. By analyzing under harmonic excitation, the proposed TMDI-TIBD shows better control performance and stronger robustness compared to TMD and TMDI, particularly when enhanced with larger tuned-mass and inertance-mass ratios. Furthermore, when the sum of the tuned-mass ratio μ and the inertance-mass ratio β_1 of TMDI-TIBD is equal to the tuned-mass ratio of the TMD, TMDI-TIBD also shows better control for both structural response and tuned-mass stroke. Compared with TMDI, TMDI-TIBD provides better control over structural vibration but has a larger tuned-mass stroke. This improvement is especially evident in lightly damped structures. In summary, TMDI-TIBD's advantage over the TMD results from the mass-amplification effect of the inerter and the double-tuning effect of the TIBD, while the enhancement of TMDI-TIBD over TMDI is chiefly dominated by the double-tuning effect of the supplemented TIBD.
3. Introducing TMDI-TIBD into a BIS shows significant enhancement compared to a conventional TMD, not only reducing the tuned-mass demand but also achieving better control of the BIS's responses and tuned-mass stroke. Compared with the TMDI strategy, TMDI-TIBD slightly improves control of the BIS's displacement and acceleration responses, albeit at the cost of a somewhat larger tuned-mass stroke. Due to the longer structural natural period of the BIS, resonant response under seismic excitation is

greatly avoided, making TMDI-TIBD's advantage over TMDI less prominent. To summarize, the advantage of the TMDI-TIBD strategy in a BIS excited by ground motions is dominated by the mass-amplification effect of the inerter.

In conclusion, the proposed TMDI-TIBD strategy has shown higher control performance, stronger control robustness, and lower tuned mass demand in the structures analyzed under harmonic and seismic excitation. Future work will focus on the design of mechanical construction, the experimental performance assessment and an in-depth analysis of TMDI-TIBD in high-rise buildings to reduce wind-induced structural vibrations.

CRediT authorship contribution statement

Xiaoyu Bai: Writing – original draft, Methodology, Investigation, Conceptualization. **Qigang Liang:** Writing – review & editing, Methodology, Funding acquisition. **Luyu Li:** Writing – review & editing, Supervision. **Breiffni Fitzgerald:** Supervision. **Jinping Ou:** Supervision.

Declaration of competing interest

The authors declare that they have no known competing financial interests or personal relationships that could have appeared to influence the work reported in this paper.

Acknowledgments

This work was supported in part by National Natural Science Foundation of China under Grant Number 52308305, the Chinese-Croatian Scientific and Technological Cooperation Project under Grant Number 10–20, and the Liaoning Provincial Natural Science Foundation under Grant Number 2023-BSBA-060. The first author gratefully acknowledges the support of China Scholarship Council during her visit to Trinity College Dublin (TCD).

Appendix A. Expressions of $\boldsymbol{A}, \boldsymbol{B}, \boldsymbol{C}, \boldsymbol{D}$

For TMDI-TVMD:

$$
\begin{aligned}
A^2 &= \left(\gamma^4 - f_1^2\gamma^2\left(1+\mu+f_t^2\left(1+\beta_t+\mu\beta_t\right)\right) + f_t^2 f_1^4 (1+\mu)\right)^2 \\
B^2 &= 4\zeta_t^2 f_1^2 \gamma^2 \beta_t^2 f_t^2 \left(-\gamma^2 + f_1^2(1+\mu)\left(1+\beta_t f_t^2\right)\right)^2 \\
C^2 &= \left(-\gamma^6 + \left(1 + f_t^2 f_1^2 + f_1^2\left(1+\beta_1+\mu\right) + \beta_t f_t^2 f_1^2\left(1+\mu+\beta_1\right)\right)\gamma^4\right. \\
&\quad \left. - \left(f_1^2 + f_t^2 f_1^2\left(1+\beta_t\right) + f_t^2 f_1^4\left(1+\beta_1+\mu\right)\right)\gamma^2 + f_t^2 f_1^4\right)^2 \\
D^2 &= 4\zeta_t^2 f_1^2 \gamma^2 \beta_t^2 f_t^2 \left(\gamma^4 - \left(1+f_1^2\left(1+\beta_t f_t^2\right)\left(1+\beta_1+\mu\right)\right)\gamma^2\right. \\
&\quad \left. + f_1^2\left(1+\beta_t f_t^2\right)\right)^2
\end{aligned}
$$

For TMDI-TID:

$$
\begin{aligned}
A^2 &= \left(\gamma^4 - f_1^2\gamma^2\left(1+\mu+f_t^2\left(1+\beta_t+\mu\beta_t\right)\right) + f_t^2 f_1^4 (1+\mu)\right)^2 \\
B^2 &= 4\zeta_t^2 f_1^2 \gamma^2 \beta_t^2 f_t^2 \left(-\left(1+\beta_t+\mu\beta_t\right)\gamma^2 + f_1^2(1+\mu)\right)^2 \\
C^2 &= \left(-\gamma^6 + \left(1 + f_t^2 f_1^2 + f_1^2\left(1+\beta_1+\mu\right) + \beta_t f_t^2 f_1^2\left(1+\beta_1+\mu\right)\right)\gamma^4\right. \\
&\quad \left. - \left(f_1^2 + f_t^2 f_1^2\left(1+\beta_t\right) + f_t^2 f_1^4\left(1+\beta_1+\mu\right)\right)\gamma^2 + f_t^2 f_1^4\right)^2 \\
D^2 &= 4\zeta_t^2 f_1^2 \gamma^2 \beta_t^2 f_t^2 \left(\left(1+\beta_t\left(1+\beta_1+\mu\right)\right)\gamma^4\right. \\
&\quad \left. - \left(1+\beta_t+f_1^2\left(1+\beta_1+\mu\right)\right)\gamma^2 + f_1^2\right)^2
\end{aligned}
$$

Appendix B. Expressions of $\boldsymbol{a}, \boldsymbol{b}, \boldsymbol{c}, \boldsymbol{d}, \boldsymbol{e}, \boldsymbol{a}', \boldsymbol{b}', \boldsymbol{c}', \boldsymbol{d}', \boldsymbol{e}'$

Minimizing displacement response amplitude

For TMDI-TVMD:

$$
\begin{aligned}
a' &= H_d^2 \\
b' &= -2H_d^2\left(1+f_1^2\left(1+\mu+\beta_1\right)\left(1+\beta_t f_t^2\right)\right) \\
c' &= -1 + H_d^2 + 2H_d^2 f_1^2\left(1+\beta_t f_t^2\right) + 2H_d^2 f_1^2\left(1+\mu+\beta_1\right)\left(1+\beta_t f_t^2\right) \\
&\quad + H_d^2 f_1^4\left(1+\mu+\beta_1\right)^2\left(1+\beta_t f_t^2\right)^2 \\
d' &= 2f_1^2\left(1+\beta_t f_t^2\right)\left(1+\mu-H_d^2-f_1^2 H_d^2\left(1+\beta_t f_t^2\right)\left(1+\beta_1+\mu\right)\right) \\
e' &= H_d^2 f_1^4\left(1+\beta_t f_t^2\right)^2 - f_1^4(1+\mu)^2\left(1+\beta_t f_t^2\right)^2
\end{aligned}
$$

For TMDI-TID:

$$
\begin{aligned}
a' &= H_d^2\left(1+\beta_t\left(1+\mu+\beta_1\right)\right)^2 \\
b' &= -2H_d^2\left(1+\beta_t+f_1^2\left(1+\beta_1+\mu\right)+\beta_t\left(1+\beta_1+\mu\right)+\beta_t^2\left(1+\beta_1+\mu\right)\right. \\
&\quad \left. + \beta_t f_1^2\left(1+\beta_1+\mu\right)^2\right) \\
c' &= -\left(1+\beta_t+\mu\beta_t\right)^2 + H_d^2\left(\left(1+\beta_t\right)^2 + f_1^4\left(1+\mu+\beta_1\right)^2\right. \\
&\quad \left. + 2f_1^2\left(2+\mu+\beta_1+2\beta_t\left(1+\mu+\beta_1\right)\right)\right) \\
d' &= 2f_1^2\left((1+\mu)\left(1+\beta_t+\mu\beta_t\right) - H_d^2\left(1+\beta_t+f_1^2\left(1+\mu+\beta_1\right)\right)\right) \\
e' &= f_1^4\left(H_d^2-(1+\mu)^2\right)
\end{aligned}
$$

Minimizing acceleration response amplitude

For TMDI-TVMD:

$$
\begin{aligned}
a &= 2 \\
b &= -2\left(1+f_1^2\left(2(1+\mu)+\beta_1+f_t^2\left(1+\beta_t\left(2+2\mu+\beta_1\right)\right)\right)\right) \\
c &= 2f_1^2\left(2+\mu+f_t^2\left(1+\beta_t(2+\mu)\right)\right) + f_1^4\left(2(1+\mu)\left(1+\beta_1+\mu\right)\right. \\
&\quad + 2f_t^2\left(\beta_1\left(1+2\beta_t(1+\mu)\right)+2(1+\mu)\left(1+\beta_t+\mu\beta_t\right)\right) \\
&\quad \left. + \beta_t f_t^8\left(\beta_1\left(1+2\beta_t(1+\mu)\right)+2(1+\mu)\left(1+\beta_t+\mu\beta_t\right)\right)\right) \\
d &= f_1^4\left(-2(1+\mu)-2f_t^2\left(2+\mu+2\beta_t(1+\mu)+f_1^2(1+\mu)\left(1+\beta_1+\mu\right)\right)\right. \\
&\quad \left. - \beta_t f_t^4\left(2+\mu+2\beta_t(1+\mu)+2f_1^2(1+\mu)\left(1+\beta_1+\mu\right)\right)\right) \\
e &= 2f_t^2 f_1^6(1+\mu)\left(1+\beta_t f_t^2\right)
\end{aligned}
$$

$$
\begin{aligned}
a' &= \left(H_a^2-2\right)H_a \\
b' &= -2\left(H_a-1\right)^2 + 2f_1^2(1+\mu)\left(1+\beta_t f_t^2\right) \\
&\quad - 2f_1^2\left(H_a-1\right)^2\left(1+\beta_1+\mu\right)\left(1+\beta_t f_t^2\right) \\
c' &= \left(H_a-1\right)^2 + 2f_1^2\left(H_a-1\right)^2\left(1+\beta_t f_t^2\right) \\
&\quad - f_1^4\left(1+\beta_t f_t^2\right)^2(1+\mu)^2 + 2f_1^2\left(H_a-1\right)^2\left(1+\beta_t f_t^2\right)\left(1+\beta_1+\mu\right) \\
&\quad + f_1^4\left(H_a-1\right)^2\left(1+\beta_t f_t^2\right)^2\left(1+\beta_1+\mu\right)^2 \\
d' &= 2f_1^2\left(H_a-1\right)^2\left(1+\beta_t f_t^2\right)\left(-1-f_1^2\left(1+\beta_t f_t^2\right)\left(1+\beta_1+\mu\right)\right) \\
e' &= f_1^4\left(H_a-1\right)^2\left(1+\beta_t f_t^2\right)^2
\end{aligned}
$$

For TMDI-TID:

$$
\begin{aligned}
a &= 2+\beta_t\left(2\mu+2+\beta_1\right) \\
b &= -2-\beta_t(2+\mu) - 2f_1^2\left(2+\beta_1+\beta_t+\beta_1\beta_t(1+\mu)+2\mu\left(1+\beta_t\right)+\beta_t\mu^2\right. \\
&\quad \left. + f_t^2\left(1+\beta_t+\mu\beta_t\right)\left(1+\beta_t\left(1+\mu+\beta_1\right)\right)\right) \\
c &= 2f_1^2\left(2+\beta_t+\mu+\mu\beta_t+f_t^2\left(1+\beta_t\right)\left(1+\beta_t+\mu\beta_t\right)\right. \\
&\quad \left. + f_1^2\left((1+\mu)\left(1+\beta_1+\mu\right)\right)\right) \\
&\quad + f_1^2 f_t^4\left(\beta_1+2\beta_1\beta_t(1+\mu)+2(1+\mu)\left(1+\beta_t+\mu\beta_t\right)\right) \\
d &= f_1^4\left(-2(1+\mu)-2f_t^2\left(2+\mu+2\beta_t(1+\mu)+f_1^2(1+\mu)\left(1+\beta_1+\mu\right)\right)\right) \\
e &= 2f_t^2 f_1^6(1+\mu)
\end{aligned}
$$

$$
\begin{aligned}
a' &= H_a^2 + 2H_a^2\beta_t\left(1+\beta_1+\mu\right) + H_a^2\beta_t^2\left(1+\beta_1+\mu\right)^2 - \left(1+\beta_t+\mu\beta_t\right)^2 \\
b' &= -2H_a^2 - 2H_a^2\beta_t - 2f_1^2 H_a^2\left(1+\beta_1+\mu\right) \\
&\quad - 2H_a^2\beta_t\left(1+\beta_1+\mu\right) - 2H_a^2\beta_t^2\left(1+\beta_1+\mu\right) - 2f_1^2 H_a^2\beta_t\left(1+\beta_1+\mu\right)^2 \\
&\quad + 2f_1^2(1+\mu)\left(1+\beta_t+\mu\beta_t\right)
\end{aligned}
$$

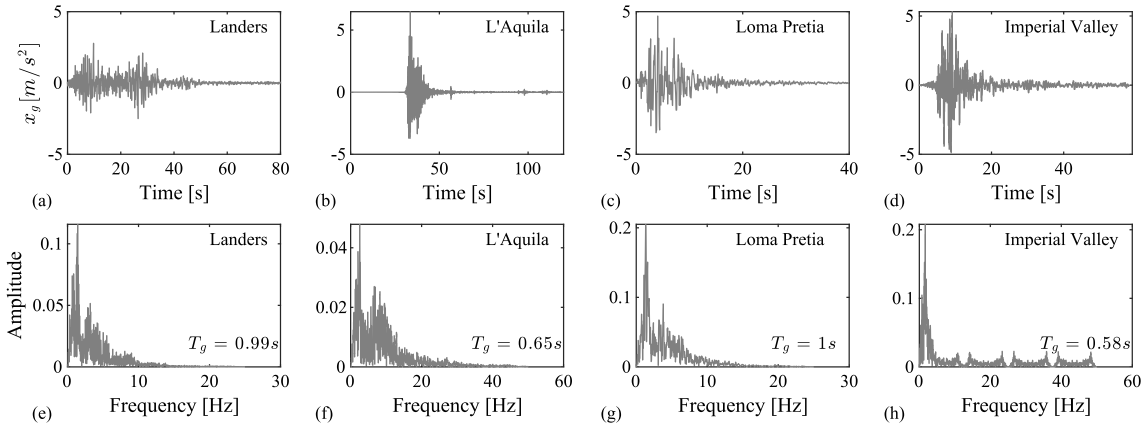

Fig. C1. (a)–(d) Time history curves and the corresponding, (e) and (f) Fourier spectrum of the used ground motions.

$$
\begin{aligned}
c' &= H_a^2 + 2f_1^2 H_a^2 + 2H_a^2\beta_t + H_a^2\beta_t^2 - f_1^4(1+\mu)^2 + 2f_1^2 H_a^2\left(1+\beta_1+\mu\right) \\
&\quad + 4f_1^2 H_a^2\beta_t\left(1+\beta_1+\mu\right) + f_1^4 H_a^2(1+\beta_1+\mu)^2 \\
d' &= -2f_1^2 H_a^2\left(1+\beta_t+f_1^2\left(1+\beta_1+\mu\right)\right) \\
e' &= H_a^2 f_1^4
\end{aligned}
$$

Appendix C. Information of used ground motions

See Fig. C1.

References

[1] Frahm H. Device for damping vibrations of bodies. US Patent 0989958; 1909.
[2] Den Hartog JP. Mechanical vibrations. New York: Dover Publications, Inc; 1985.
[3] Kwon HC, Kim MC, Lee IW. Vibration control of bridges under moving loads. Comput Struct 1998;66(4):473–80. https://doi.org/10.1016/S0045-7949(97)00087-4
[4] Kareem A, Kijewski T, Tamura Y. Mitigation of motions of tall buildings with specific examples of recent applications. Wind Struct 1999;2(3):201–51. https://doi.org/10.12989/WAS.1999.2.3.201
[5] Rana R, Soong TT. Parametric study and simplified design of tuned mass dampers. Eng Struct 1998;20(3):193–204. https://doi.org/10.1016/S0141-0296(97)00078-3
[6] Liu M, Li S, Wu T, Li Y, Meng H, Chen Z. Eddy-current tuned mass dampers for mitigation of wind-induced response of the Noor III solar tower: design, installation, and validation. J Struct Eng 2021;147(12):05021009. https://doi.org/10.1061/(ASCE)ST.1943-541X.0003180
[7] Lu X, Zhang Q, Weng D, Zhou Z, Wang S, Mahin SA, et al. Improving performance of a super tall building using a new eddy-current tuned mass damper. Struct Control Health Monit 2017;24(3):e1882. e1882 STC-15-0170.R1. https://doi.org/10.1002/stc.1882
[8] Song GB, Zhang P, Li LY, Singla M, Patil D, Li HN, et al. Vibration control of a pipeline structure using pounding tuned mass damper. J Eng Mech 2016;142(6):04016031. https://doi.org/10.1061/(ASCE)EM.1943-7889.0001078
[9] Lu Z, Wang Z, Masri SF, Lu X. Particle impact dampers: past, present, and future. Struct Control Health Monit 2018;25(1):e2058. e2058 STC-17-0042.R1. https://doi.org/10.1002/stc.2058
[10] Matta E. A novel bidirectional pendulum tuned mass damper using variable homogeneous friction to achieve amplitude-independent control. Earthq Eng Struct Dyn 2019;48(6):653–77. https://doi.org/10.1002/eqe.3153
[11] Liang Q, Li L. Optimal design for a novel inerter-based clutching tuned mass damper system. J Vib Control 2020;26(21–22):2050–59. https://doi.org/10.1177/1077546320910532
[12] Smith MC. Synthesis of mechanical networks: the inerter. IEEE Trans Autom Control 2002;47(10):1648–62. https://doi.org/10.1109/TAC.2002.803532
[13] Lazar IF. Using an inerter-based device for structural vibration suppression. Earthq Eng Struct Dyn 2014;43(8):1129–47. https://doi.org/10.1002/eqe.2390
[14] Ikago K, Saito K, Inoue N. Seismic control of single-degree-of-freedom structure using tuned viscous mass damper. Earthq Eng Struct Dyn 2012;41(3):453–74. https://doi.org/10.1002/eqe.1138
[15] Liang Q, Bai X, Yu D, Li L, Ou J. Dynamic performance of structures with clutching inertia-damping system: theoretical study. Earthq Eng Struct Dyn 2024;53(3):1345–62. https://doi.org/10.1002/eqe.4072
[16] Liang Q, Yu D, Wei J, Li L, Ou J. Theoretical study of a novel resettable-inertia damper: dynamic modeling, equivalent linearization, and performance assessment. Earthq Eng Struct Dyn 2024;11(53):eqe.4186. https://doi.org/10.1002/eqe.4186
[17] Tai Y, Cheng L, Liu L, Bao H. Optimal design and performance analysis of a tuned negative-stiffness inerter mass damper for vibration control systems. Structures 2025;73:108163. https://doi.org/10.1016/j.istruc.2024.108163
[18] Garrido H, Curadelli O, Ambrosini D. Improvement of tuned mass damper by using rotational inertia through tuned viscous mass damper. Eng Struct 2013;56:2149–53. https://doi.org/10.1016/j.engstruct.2013.08.044
[19] Hu Y, Chen MZ. Performance evaluation for inerter-based dynamic vibration absorbers. Int J Mech Sci 2015;99:297–307. https://doi.org/10.1016/j.ijmecsci.2015.06.003
[20] Barredo E, Blanco A, Colín J, Penagos VM, Abúndez A, Gerardo Vela L, et al. Closed-form solutions for the optimal design of inerter-based dynamic vibration absorbers. Int J Mech Sci 2018;144:41–53. https://doi.org/10.1016/j.ijmecsci.2018.05.025
[21] Bai X, Liang Q, Huo L. Vibration control of beam-model using tuned inerter enhanced TMD. J Sound Vib 2021;510:116304. https://doi.org/10.1016/j.jsv.2021.116304
[22] Zeng C, Zhang Z, Su N. Enhanced vibration control on transmission towers with rotational inertial double tuned mass dampers for seismic and wind hazards. Structures 2025;73:108326. https://doi.org/10.1016/j.istruc.2025.108326
[23] Zhang Z, Høeg C. Inerter-enhanced tuned mass damper for vibration damping of floating offshore wind turbines. Ocean Eng 2021;223:108663. https://doi.org/10.1016/j.oceaneng.2021.108663
[24] Marian L, Giaralis A. Optimal design of a novel tuned mass-damper-inerter (TMDI) passive vibration control configuration for stochastically support-excited structural systems. Probab Eng Mech 2014;38:156–64. https://doi.org/10.1016/j.probengmech.2014.03.007
[25] Pietrosanti D, De Angelis M, Giaralis A. Experimental study and numerical modeling of nonlinear dynamic response of SDOF system equipped with tuned mass damper inerter (TMDI) tested on shaking table under harmonic excitation. Int J Mech Sci 2020;184:105762. https://doi.org/10.1016/j.ijmecsci.2020.105762
[26] Giaralis A, Petrini F. Wind-induced vibration mitigation in tall buildings using the tuned mass-damper-inerter. J Struct Eng 2017;143(9):04017127. https://doi.org/10.1061/(ASCE)ST.1943-541X.0001863
[27] De Domenico D, Ricciardi G. An enhanced base isolation system equipped with optimal tuned mass damper inerter (TMDI). Earthq Eng Struct Dyn 2018;47(5):1169–92. https://doi.org/10.1002/eqe.3011
[28] De Domenico D, Ricciardi G. Improving the dynamic performance of base-isolated structures via tuned mass damper and inerter devices: a comparative study. Struct Control Health Monit 2018;25(10):e2234. https://doi.org/10.1002/stc.2234
[29] Hwang JS, Kim J, Kim YM. Rotational inertia dampers with toggle bracing for vibration control of a building structure. Eng Struct 2007;29(6):1201–08. https://doi.org/10.1016/j.engstruct.2006.08.005
[30] Makris N, Kampas G. Seismic protection of structures with supplemental rotational inertia. J Eng Mech 2016;142(11):04016089. https://doi.org/10.1061/(ASCE)EM.1943-7889.0001152
[31] Málaga-Chuquitaype C, Menendez-Vicente C, Thiers-Moggia R. Experimental and numerical assessment of the seismic response of steel structures with clutched inerters. Soil Dyn Earthq Eng 2019;121:200–11. https://doi.org/10.1016/j.soildyn.2019.03.016
[32] Thiers-Moggia R, Málaga-Chuquitaype C. Seismic protection of rocking structures with inerters. Earthq Eng Struct Dyn 2019;48(5):528–47. https://doi.org/10.1002/eqe.3147
[33] Wang FC, Hong MF, Lin TC. Designing and testing a hydraulic inerter. Proc Inst Mech Eng, Part C J Mech Eng Sci 2011;225(1):66–72. https://doi.org/10.1243/09544062JMES2199
[34] Nakamura Y, Fukukita A, Tamura K, Yamazaki I, Matsuoka T, Hiramoto K, et al. Seismic response control using electromagnetic inertial mass dampers. Earthq Eng Struct Dyn 2014;43(4):507–27. https://doi.org/10.1002/eqe.2355
[35] De Domenico D, Deastra P, Ricciardi G, Sims ND, Wagg DJ. Novel fluid inerter based tuned mass dampers for optimised structural control of base-isolated buildings. J Franklin Inst 2019;356(14):7626–49. https://doi.org/10.1016/j.jfranklin.2018.11.012
[36] Pietrosanti D, De Angelis M, Giaralis A. Experimental seismic performance assessment and numerical modelling of nonlinear inerter vibration absorber (IVA)-equipped base isolated structures tested on shaking table. Earthq Eng Struct Dyn 2021;50(10):2732–53. https://doi.org/10.1002/eqe.3469

[37] Cao L, Li C. Tuned tandem mass dampers-inerters with broadband high effectiveness for structures under white noise base excitations. Struct Control Health Monit 2019;26(4):e2319. https://doi.org/10.1002/stc.2319

[38] Djerouni S, Abdeddaim M, Elias S, Rupakhety R. Optimum double mass tuned damper inerter for control of structure subjected to ground motions. J Build Eng 2021;44:103259. https://doi.org/10.1016/j.jobe.2021.103259

[39] Zhou S, Jean-Mistral C, Chesne S. Influence of inerters on the vibration control effect of series double tuned mass dampers: two layouts and analytical study. Struct Control Health Monit 2019;26(10). https://doi.org/10.1002/stc.2414

[40] Masnata C, Di Matteo A, Adam C, Pirrotta A. Smart structures through non-traditional design of tuned mass damper inerter for higher control of base isolated systems. Mech Res Commun 2020;105:103513. https://doi.org/10.1016/j.mechrescom.2020.103513

[41] Javidialesaadi A, Wierschem NE. An inerter-enhanced nonlinear energy sink. Mech Syst Signal Process 2019;129:449–54. https://doi.org/10.1016/j.ymssp.2019.04.047

[42] Cheng Z, Palermo A, Shi Z, Marzani A. Enhanced tuned mass damper using an inertial amplification mechanism. J Sound Vib 2020;475:115267. https://doi.org/10.1016/j.jsv.2020.115267

[43] Liang Q, Li L. Analysis of the TMD enhanced base isolation system (BIS) using clutching inerter damper. In: Earth and space 2021. American Society of Civil Engineers; 2021. p. 359–67.

[44] Fahimi Farzam M, Hojat Jalali H. Tandem tuned mass damper inerter for passive control of buildings under seismic loads. Struct Control Health Monit 2022;29(9). https://doi.org/10.1002/stc.2987

[45] Khorsand S, Rofooei FR. H∞ optimum design and nonlinear seismic performance assessment of tuned-mass-damper-inerter (TMDI) supported by an auxiliary structure. Structures 2024;69:107257. https://doi.org/10.1016/j.istruc.2024.107257

[46] Warburton GB. Optimum absorber parameters for various combinations of response and excitation parameters. Earthq Eng Struct Dyn 1982;10(3):381–401. https://doi.org/10.1002/eqe.4290100304

[47] Marian L, Giaralis A. The tuned mass-damper-inerter for harmonic vibrations suppression, attached mass reduction, and energy harvesting. Smart Struct Syst 2017;19(6):665–78. https://doi.org/10.12989/SSS.2017.19.6.665

[48] Barredo E, Mendoza Larios JG, Colín J, Mayén J, Flores-Hernández AA, Arias-Montiel M. A novel high-performance passive non-traditional inerter-based dynamic vibration absorber. J Sound Vib 2020;485:115583. https://doi.org/10.1016/j.jsv.2020.115583